Assessing the impact of CO_2 equilibrated ocean alkalinity enhancement on microbial metabolic rates in an oligotrophic system

Laura Marín-Samper[1], Javier Arístegui[1], Nauzet Hernández-Hernández[1], Joaquín Ortiz[1], Stephen D. Archer[3,] Andrea Ludwig[2], Ulf Riebesell[2]

[1] Instituto de Oceanografía y Cambio Global, Universidad de Las Palmas de Gran Canaria, 35017 Telde, Spain
[2] GEOMAR Helmholtz Centre for Ocean Research Kiel, 24148 Kiel, Germany
[3] Bigelow Laboratory for Ocean Sciences, 60 Bigelow Dr., PO Box 380, East Boothbay, Maine 04544, USA

Correspondence to: Laura Marín-Samper (laura.marin@ulpgc.es), Javier Arístegui (javier.aristegui@ulpgc.es)

Abstract. Ocean Alkalinity Enhancement (OAE) is a Negative Emissions Technology (NET) that shows significant potential for climate change mitigation. By increasing the bicarbonate ion concentration in ocean water, OAE could enhance long-term carbon storage and mitigate ocean acidification. However, the side effects and/or potential co-benefits of OAE on natural planktonic communities remain poorly understood. To address this knowledge gap, a mesocosm experiment was conducted in the oligotrophic waters of Gran Canaria. A CO_2-equilibrated Total Alkalinity (TA) gradient was employed in increments of 300 $\mu mol \cdot L^{-1}$, ranging from ~2400 to ~4800 $\mu mol \cdot L^{-1}$. This study represents the first attempt to evaluate the potential impacts of OAE on planktonic communities under natural conditions. The results show that Net Community Production (NCP), Gross Production (GP), Community Respiration (CR) rates, as well as the metabolic balance (GP:CR), did not exhibit a linear response to the whole alkalinity gradient. Instead, significant polynomial and linear regression models were observed for all rates up to $\Delta TA1800$ $\mu mol \cdot L^{-1}$, in relation to the Dissolved Inorganic Carbon (DIC) concentrations. Notably, the $\Delta TA1500$ and 1800 $\mu mol \cdot L^{-1}$ treatments showed peaks in NCP shifting from a heterotrophic to an autotrophic state, with NCP values of 4 and 8 μmol O_2 kg^{-1} d^{-1}, respectively. These peaks and the optimum curve were also reflected in the phytoplankton abundance, size-fractioned chlorophyll *a* and ^{14}C uptake data. Furthermore, abiotic precipitation occurred in the highest treatment after day 21 but no impact on the measured parameters was detected. Overall, a damaging effect of CO_2-equilibrated OAE in the range applied here, on phytoplankton primary production, community metabolism and composition could not be inferred. In fact, a potential co-benefit to OAE was observed in the form of the positive curvilinear response to the DIC gradient up to the $\Delta TA1800$ treatment. Further experimental research at this scale is key to gain a better understanding of the short and long-term effects of OAE on planktonic communities.

Keywords. CDR, OAE, alkalinization, plankton, primary production, metabolic rates

1 Introduction

Limiting global warming to between 1.5ºC and 2ºC relative to preindustrial times, as stipulated in the 2015 Paris Agreement, will be necessary to avoid long-term, dangerous climatic consequences. Out of all the scenarios outlined in the fifth IPCC Assessment Report that meet this temperature target, 87% require extensive deployment of technologies to remove and sequester carbon dioxide (CO_2) from the atmosphere (Burns & Corbett, 2020; IPCC, 2018). Similarly, the Shared Socio-Economic Pathways that assume net-zero CO_2 emissions being reached by 2050, and negative emissions for the rest of this century, are the only ones in which the temperature increase is "*more likely than not*" bounded to below 2ºC (IPCC, 2022). Besides, an estimated 26% of the anthropogenic CO_2 emitted between 1750 and 2020 has been taken up by the ocean through sea-gas exchange (Friedlingstein et al., 2022), subsequently altering its chemistry (Feely et al., 1985; Orr et al., 2005). Process that is commonly known as ocean acidification (OA). This phenomenon is notorious for being a threat to a wide range of marine taxa in terms of overall survival, calcification, growth, development and abundance (Hendriks & Duarte, 2010; Kroeker et al., 2010, 2013; Wittmann & Pörtner, 2013). The implementation of Carbon Dioxide Removal (CDR) strategies will thus be crucial to timely offset the hard to abate emissions (Haszeldine et al., 2018; IPCC, 2018, 2022; National Academies of Sciences, Engineering and Medicine, 2021; Renforth et al., 2013). Yet most approaches remain understudied, particularly those focused on ocean-based CDR (Gattuso et al., 2018, 2021; Rau et al., 2012).

Ocean alkalinity enhancement (OAE) is one of the ocean-based Negative Emissions Technologies (NETs) that is presently being considered. It consists of atmospheric CO_2 removal by enhancing the ocean's carbon uptake capacity through mineral weathering (Kheshgi, 1995). It involves the dissolution of carbonate or silicate based alkaline or alkali compounds/minerals in seawater, altering the carbonate chemistry equilibrium by pushing it towards the carbonate and bicarbonate ion species. Thereby dissolved CO_2 concentration is reduced, counteracting OA while allowing for additional CO_2 uptake from the atmosphere. Model studies indicate that OAE could potentially remove between 3 and 10 Gt of atmospheric CO_2 per year (Feng et al., 2017; Harvey, 2008). Given the urgency to remove, capture, and store atmospheric CO_2 (Haszeldine et al., 2018; IPCC, 2018, 2022) and the ocean's potential to do so (Burns & Corbett, 2020), the evaluation of OAE applicability is of vital importance. Its implementation will depend on its scalability and on its environmental safety.

There are many proposed approaches for OAE deployment. For example, the supply of ground up minerals to coastal environments, the injection of alkaline solutions to, or dispersal of alkaline particles over, the surface ocean, and the electrochemical acid removal from seawater (Eisaman et al., 2023; Renforth & Henderson, 2017). In the present study we simulated a carbonate-based alkalinity addition to the open ocean surface, namely ocean liming, using a mesocosm approach. There are many model-based studies that focused on evaluating the feasibility, scalability and efficacy of this OAE approach (Butenschön et al., 2021; Caserini et al., 2021; González & Ilyina, 2016; Ilyina et al., 2013; Kheshgi, 1995; Lenton et al., 2018). But although conceptually it shows potential to mitigate OA and for CDR at global and regional scales, all the model simulations are based on a series of assumptions that remain poorly understood (Hartmann et al., 2023). This is due to the lack of focused experimental work under natural conditions.

80   Choosing a suitable approach to employ ocean liming is essential and complex. The maintenance of high alkalinity levels and thus the avoidance of alkalinity consumption through abiotic carbonate precipitation is key to ensure its CDR potential (Hartmann et al., 2023). Additionally, the type of source mineral, grinding fineness, whether it is added in its particulate form or in solution, if the latter is CO_2 equilibrated prior to addition or not, but also the presence of biogenic or abiotic particles in seawater (Moras et al., 2022), can

85   all influence the efficiency of OAE.

The simplest ocean liming deployment strategy is the direct dispersal of ground up minerals to the surface ocean (Harvey, 2008; Köhler et al., 2013). This method, however, may facilitate abiotic precipitation by supplying substrate for carbonate formation in an already supersaturated medium (Wurgaft et al., 2021). Additionally, if silicate-based (through the use of, for instance, dunite, an olivine rich mineral), it may cause

90   the release of potentially harmful dissolution by-products such as trace metals (Bach et al. 2019; Ferderer et al. 2022; Montserrat et al. 2017; Meysman and Montserrat 2017). Thus, despite being the simplest, it may not be the most suitable approach. The impacts on biota of different OAE strategies may also depend on the associated changes to the carbonate chemistry. This is especially true for non-CO_2 equilibrated OAE deployment scenarios where pCO_2 would be decreased, and thus pH more heavily altered than when

95   employing an equilibrated approach (Bach et al., 2019; Paul & Bach, 2020; Chen et al., 1994; Giordano et al., 2005; Riebesell et al., 1993).

As a first step, to test the effect of an increment in total alkalinity (TA) and dissolved inorganic carbon (DIC), and to examine TA stability, we deployed an alkalinity gradient with carbonate-based air equilibrated solutions. Therefore, our TA manipulation did not contain any associated, and potentially

100   harmful, dissolution by-products. This way simulating the alkalinity levels reached as one gradually moves away from a hypothetical OAE point source, under a best-case scenario. Changes in metabolic rates, primary production, chlorophyll a concentration and community composition, associated with the alkalinity gradient applied, were monitored. The goal was thus to detect possible environmental impacts and alkalinity thresholds. No major effects were expected since the carbonate chemistry parameters that are believed to

105   drive phytoplankton growth, CO_2 and H^+ concentration (Paul & Bach, 2020), remained unaltered and moderately decreased respectively.

2 Materials and Methods

2.1 Experimental Design and Sampling

110   The experiment (KOSMOS Gran Canaria 2021) was set up at the Oceanic Platform of the Canary Islands' (PLOCAN) pier in the Taliarte harbour, Gran Canaria (Canary Islands, Spain), from September 14th to October 16th, 2021. Nine mesocosms were deployed. They were supported by floating frames with joined flexible bags of 4m in length that were suspended and enclosed at the bottom with a conical sediment trap (Goldenberg et al., 2022; Supp. Fig. S1). Mesocosms were simultaneously filled up on September 10th,

115   2021, with pre-filtered (3 mm) seawater pumped from nearby offshore waters (from the integrated water column going from 2-12 m depth) with a peristaltic pump (14 m^3 h^{-1}, KUNZ SPF60, Flexodamp FD-50). Seawater was distributed equally across all mesocosms using a digital flow meter. The attained final volumes ranged between 8001 - 8051 L.

To examine the effects of an increment in TA, we applied an alkalinity gradient of nine steps in increments of 300 µmol · L^{-1}, with air equilibrated Na_2CO_3 and $NaHCO_3$ stock solutions. The latter were prepared by adding the corresponding weighed salts to 22L of deionized water that contained the difference in TA between the ambient and the target levels. The applied gradient is displayed in Table 1. The averages of the measured (see section 2.2) TA and DIC are shown in italics, and were used to calculate the rest of the carbonate chemistry parameters using CO2SYS v2.1 software (Lewis & Wallace, 1998). Lueker et al.'s (2000) carbonate dissociation constants (K_1 and K_2), and the boron from Uppström (1974), were the constants employed for the mentioned calculation. Salinity was set to 36.55 up to day 17, and to 37 from day 19 onwards.

Table 1. Averages for the whole experiment of the measured TA and DIC (italics), and theoretical values obtained through CO2SYS v2.1 software for the rest of the carbonate system parameters, for each mesocosm (MK). The first column constitutes the colour code followed henceforth. TA, DIC, HCO_3^- and CO_3^{2-} concentration units correspond to µmol · L^{-1}, pCO_2 is in µatm.

MK	TA	DIC	pH	pCO_2	HCO_3^-	CO_3^{2-}	Ω_{Ca}	Ω_{Ar}
5	*2423.8*	*2119.0*	8.030	422.1	1890.1	216.7	5.1	3.4
1	*2706.4*	*2349.8*	8.059	434.9	2066.1	254.1	6.0	3.9
7	*2902.8*	*2537.4*	8.087	432.7	2210.3	291.8	6.9	4.5
4	*3147.5*	*2710.6*	8.116	432.1	2362.9	334.9	7.9	5.2
9	*3403.1*	*2966.0*	8.136	439.9	2528.5	377.8	8.9	5.9
3	*3634.6*	*3156.5*	8.160	437.0	2661.8	424.2	10.0	6.6
6	*3864.6*	*3286.1*	8.182	434.3	2790.6	472.3	11.2	7.3
2	*4227.5*	*3568.1*	8.199	441.1	2957.6	520.5	12.3	8.1
8	*4299.4*	*3633.4*	8.201	455.5	3074.0	546.0	12.9	8.5

Mesocosms were set out in a pseudo random order along the pier. Custom-made samplers, constructed with 2.5 m long polypropylene tubing with a valve at each end, and a 5 L internal volume, were used to collect depth-integrated samples. These were collected every two days for a 33-day period. For further details on all activities conducted throughout the experiment including CTD and net tows, sediment trap pumping, mesocosm cleaning and overall maintenance, refer to Supp. Fig. S2.

2.2 TA and DIC measurements

TA and DIC samples were collected directly from the custom-made samplers into 250 mL glass flasks, allowing for substantial overflow and no headspace to avoid contamination. The samples were sterile filtered (0.2 µm, SARSTEDT, Nümbrecht, Germany) with a peristaltic pump. TA concentrations were determined by potentiometric titration using a Metrohm 862 Compact Titrosampler with HCl 0.05 M as the titrant, Aquatrode Plus (Pt1000), and 907 Titrando unit as in Chen et al., 2022. DIC concentrations were measured using an AIRICA system (Marianda, Kiel, Germany; see Gafar & Schulz, 2018, and Taucher et

al., 2017) with a differential gas analyzer (LI-7000, LI-COR Biosciences GmbH, Bad Homburg, Germany) at room temperature and within 12 h.

2.3 Metabolic Rates through Oxygen Production and Consumption

150 Gross Production (GP), Net Community Production (NCP), and Community Respiration (CR) rates were determined by oxygen production and consumption in calibrated 125 mL nominal volume soda lime glass bottles following the Winkler method and the recommendations from Carpenter (1966), Bryan et al. (1976), and Grasshof et al. (1999). Polycarbonate bottles were filled with 4.5 L of seawater per mesocosm on each sampling day and brought to the lab. Out of these samples, twelve soda lime bottles per mesocosm were

155 first rinsed with sample water and then randomly filled, allowing ample overflow, using a silicone tube with an attached 280 µm mesh on one end. The lids were then carefully placed, and each individual bottle was checked to be bubble free. Four subsamples per mesocosm were fixed at the moment of collection, "initials", through the addition of 1 mL of a manganese sulphate ($MnSO_4$) solution and 1 mL of a sodium iodide (NaI) based alkaline solution, in this order. They were later covered with a blackout piece of fabric

160 and stored in a rack underwater. Another four bottles were incubated in the "dark", and the remaining four were incubated under "light" conditions. The "dark" ones were set inside light proof bags, which were then placed in a black opaque box. The "light" ones were randomly distributed inside clear methacrylate boxes, which were covered with a blue foil (172 Lagoon Blue foil, Lee filters, Burbank, USA) to better simulate the light spectrum of the water column. The boxes containing the light and dark bottles, and the rack with

165 the initials, were placed in an outside pool found in the Parque Científico Tecnológico Marino of Taliarte, fed with a constant flow of seawater from the Taliarte pier. Data loggers (HOBO UA-002-64, Australia/New Zealand) were put inside the incubators to monitor the temperature (approximately 24.3 and 23.8 °C during the day and night, respectively) and light (ranging from 0.25 to approximately 2313.15 µmol photons m^{-2} s^{-1} on average) conditions throughout the experiment. After an incubation period of 24 hours,

170 all samples were fixed and left to sediment for at least 2 hours. Finally, samples were acidified with 1 mL of 5 M sulphuric acid (H_2SO_4) right before being analysed with an automated titration system, with colorimetric end-point detection (Dissolved Oxygen Analyzer, SIS Schwentinental, Germany), using a 0.25 M sodium thiosulphate solution ($Na_2S_2O_3 * 5H_2O$) as the titrant. The mean of each set of four replicates was used to calculate CR, NCP, and GP rates, using the following Eq. (1), Eq. (2) and Eq. (3) respectively:

175

$$CR \; [\mu mol \; L^{-1}h^{-1}] = \frac{Conc_I - Conc_D}{h_D} \qquad (1)$$

$$NCP \; [\mu mol \; L^{-1}h^{-1}] = \frac{Conc_L - Conc_I}{h_L} \qquad (2)$$

180
$$GP \; [\mu mol \; L^{-1}h^{-1}] = CR + NCP \qquad (3)$$

where $Conc_I$, $Conc_D$ and $Conc_L$ correspond to the mean oxygen concentration of the initial, dark, and light samples, respectively. T stands for incubation time in hours. The metabolic balance was later calculated by dividing the obtained GP by CR.

2.4 Size-fractionated Primary Production through ^{14}C uptake

Primary production (PP) in pico (0.2-2 µm), nano (2-20 µm), and micro (20-280 µm) size fractions were measured following a modified version of the approach by Cermeño et al. (2012). Samples from each mesocosm were taken into 10 L High Density Polyethylene (HDPE) canisters and transported to the GOB laboratories every two sampling days. Four culture flasks (Sarstedt TC Flask d15, Nümbrecht, Germany) per mesocosm were filled up to the bottle neck (70 mL) and spiked with 80 µL (0.296 MBq) of a ^{14}C-labeled sodium bicarbonate (NaH^{14}CO$_3$, Perkin Elmer, Waltham, USA) stock solution (3.7 MBq mL^{-1}). Prior to ^{14}C inoculation, samples were prefiltered through a 280 µm mesh to exclude most of the zooplankton fraction. Each flask was then closed and gently homogenized. All culture flasks were incubated for 24 h in an environmental chamber (Aralab FitoClima 600 Bio Chamber, Lisbon, Portugal) at *in situ* light (12 h light-dark cycle with a mean daily PAR intensity of ~500 µmol photons m^{-2} s^{-1}) and temperature (21 - 24 °C depending on the temperature in the mesocosms on each sampling day). One out of the four culture flasks per mesocosm was incubated inside a light-proof bag to prevent photosynthesis.

After incubation, all samples were sequentially filtered on a circular filtration manifold (Oceomic, Fuerteventura, Spain) under low vacuum pressure (<200 mbar) through polycarbonate membrane filters with pore sizes of 20 µm (top), 2 µm (middle) and 0.2 µm (bottom) (DHI GVS 20 µm, Hørsholm, Denmark, Whatman Nuclepore 2 µm & 0.2 µm, Maidstone, UK). The manifold allowed to collect the filtrate in 120 mL HDPE bottles. The filters were placed in 5 mL scintillation vials (Sarstedt HDPE Mini-vial, Nümbrecht, Germany), while 5 mL of the filtrates were transferred to 20 mL scintillation vials (Sarstedt HDPE Scintillation vial, Nümbrecht, Germany) for dissolved organic carbon production (PP$_{DOC}$) determination.

To remove the remaining inorganic ^{14}C, all samples were acidified. To do so, the 5 mL vials with the filters were placed inside a desiccator and exposed to fuming hydrochloric acid (HCl 37 %) for 24 h. Whilst 100 µL of hydrochloric acid (HCl 17.5 %) were added to the filtrate subsamples and placed on an orbital oscillator at 60 rpm, also for 24 h.

After acidifying, filters were pushed into the vials and 3.5 and 10 mL of scintillation cocktail (Ultima Gold XR, Perkin Elmer, Waltham, USA) were added to the filters and the liquid samples, respectively. All vials were vigorously shaken and left for an additional 24 h in the dark before being measured with a scintillation counter (Beckman LS-6500, Brea, USA). The counted disintegrations per minute (DPM) were used to calculate primary production rates [µg C L^{-1} h^{-1}] using the following Eq. (4):

$$PP = \frac{V_S}{V_F} \cdot \frac{DIC \cdot (DPM_S - DPM_D)}{DPM_A \cdot t_i} \tag{4}$$

where V_S = sample volume (L), V_F = filtered volume (L), DPM_S = sample disintegrations per minute, DPM_D = dark-incubated sample disintegrations per minute, DIC = dissolved inorganic carbon (µmol C L^{-1}), DPM_A = initially added ^{14}C in disintegrations per minute, and t_i= time of incubation (h).

The average of the triplicates was used to calculate the final PP rates. The three size fractions were summed up to calculate the particulate organic carbon production (PP$_{POC}$). Moreover, the Eq. (5) below was utilized to calculate the Percentage of Extracellular organic carbon Release (PER):

$$PER\ (\%) = \frac{PP_{DOC}}{PP_{POC} + PP_{DOC}} \cdot 100 \qquad (5)$$

2.5 Size-fractionated Chlorophyll *a*

Chlorophyll *a* (Chl*a*) samples for each mesocosm were collected into 500 mL dark bottles from the same 10 L canisters as PP. Samples were sequentially filtered through superimposed Polycarbonate filters of 20 μm, 2 μm and 0.2 μm pore size (DHI GVS 20 μm, Hørsholm, Denmark, Whatman Nuclepore 2 μm and 0.2 μm, Maidstone, UK). The filters were stored at -20 °C while pending analysis. The pigment was extracted by submerging the filters in 10 mL of acetone (90%) at -20 °C for 24 h. The extracts were analyzed using a benchtop fluorometer Turner Design AU-10 (San Jose, USA) as in Welschmeyer (1994). Total Chl*a* concentration was determined by adding up the three size fractions.

2.6 Prokaryotic and Eukaryotic Abundances

Duplicate flow cytometry samples were collected every two days and ran in vivo each day. A CytoSense (Cytobuoy, Woerden, Netherlands) flow cytometer was used, and the default software (Cytoclus) was employed to differentiate the phytoplankton population clusters based on red, orange, and green fluorescence as well as forward and side scatter (Dubelaar & Gerritzen, 2000).

2.7 Data Analysis

The experiment was divided into two phases (I: days 5-19, II: days 21-33; the reasons for this division are explained in the results section). All parameters were analyzed in relation to the alkalinity gradient deployed using simple linear regressions. Additionally, in the parameters that showed a potential curvilinear trend in relation to the TA/DIC gradient, linear and polynomial regression models were also fitted excluding the two highest treatments. For these parameters, in order to avoid over-fitting, cross validation was used to assess the polynomial model's performance to pick the best-fitting model order. DIC was chosen as the predictor variable for the latter. Averages of the response variables for each phase and for the entirety of the experiment, in both cases excluding the days prior to the TA addition, were used. Assumptions of normality were tested using q-q and Shapiro-Wilk tests on test residuals. Data analyses were performed using RStudio (2022.02.3 Build 492; packages stats, ggplot2 v3.3.5; Wickham, 2016).

3 Results

3.1 Carbonate chemistry temporal development and phase determination

The TA gradient in increments of 300 μmol · L^{-1} was attained, and DIC and TA were stable up to day 21 (Figure 1.A). The experimental period up to that day, 5 – 19, was differentiated and designated as phase I (< 12 days after the TA addition). After day 21, termed phase II (>14 days after the TA addition), indirect abiotic precipitation occurred in the highest treatment, Δ2400 μmol · L^{-1}. Precipitates were visibly forming on the mesocosm walls by day 28, a process that advanced quite rapidly during the 6 days after cleaning. The precipitation process lasted until the end of the experiment and led to a TA and DIC loss of ~ 293.7 μmol · L^{-1} and 175.3 μmol· L^{-1}, respectively (Figure 1.A and B).

After the alkalinity addition on day 4, the pH varied slightly according to the gradient applied ranging from 8.03 in the control to 8.2 in the highest treatment (Figure 1.C). CO_2 partial pressure did not vary alongside the TA gradient due to the equilibrated nature of the alkalinity manipulation (Figure 1.D). However, the estimated pCO_2 in the highest treatment in phase II increased from ~ 450 in phase I, to a maximum of 541 µatm by day 33 due to the triggered calcification process (ΔTA 2400 µmol · L^{-1}). It was ~20 µatm higher than the rest of the treatments starting on day 27, increasing towards the end of the experiment, when it was ~100 µatm greater than ambient levels (Figure 1.D). Because of the increase in pCO_2 in this treatment in phase II, pH dropped from 8.23 on day 18, down to a minimum of 8.16 at the end of the experiment (Figure 1. C and D).
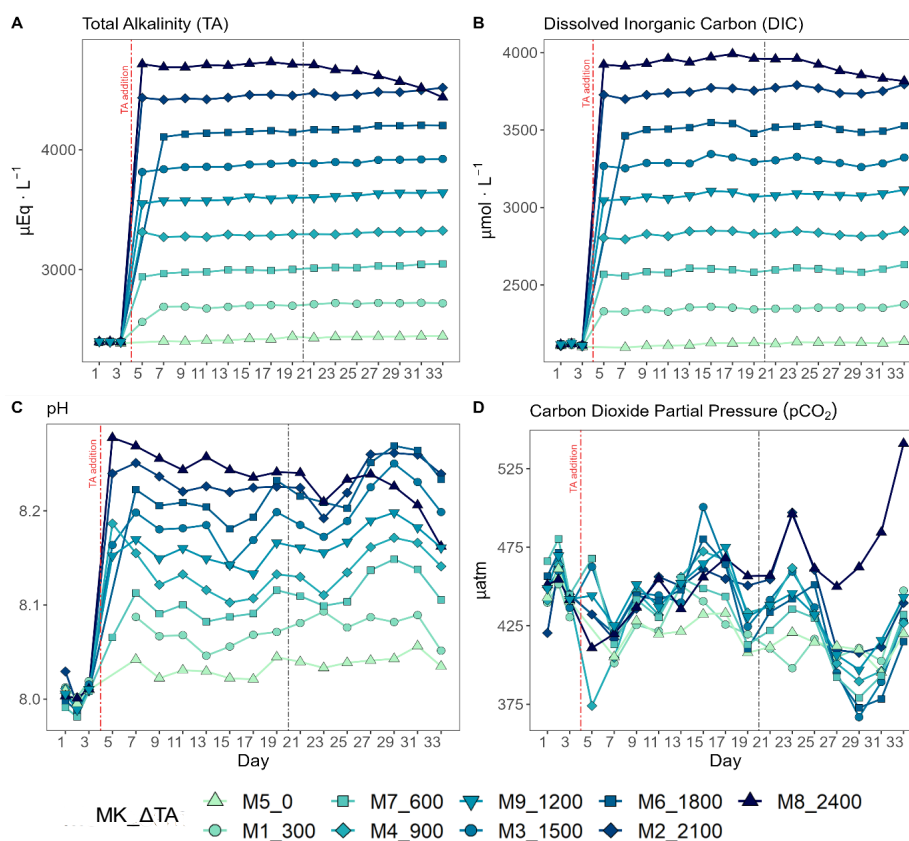
Figure 1. Temporal development of A) Total Alkalinity (TA), B) Dissolved Inorganic Carbon (DIC), C) pH and D) pCO₂ throughout the entire experiment for each mesocosm (MK) and treatment (ΔTA)

3.2 Primary production and metabolic balance

Another reason for the mentioned phase delimitation is the increase in production and Chl*a* concentration in certain intermediate treatments past day 20 when compared to phase I (Figure 2). The separation in these two phases was decided upon also to ease interpretation of the system's response. Overall, NCP, GP, and the metabolic balance (GP:CR) show similar developments. All metabolic rates behaved differently in the

two phases (Figure 2.A, B and C). In the first phase, CR accounted for most of the GP, while NCP was for

280   the most part negative (more respiration than oxygen production; Figure 2.B and D). In contrast, a peak in

GP and NCP rates occurred at Δ1500 and Δ1800 during the second phase, showing 2 and 3-fold increased

GP, respectively. Autotrophy was also observed in the Δ600 and Δ900 treatments during this phase although
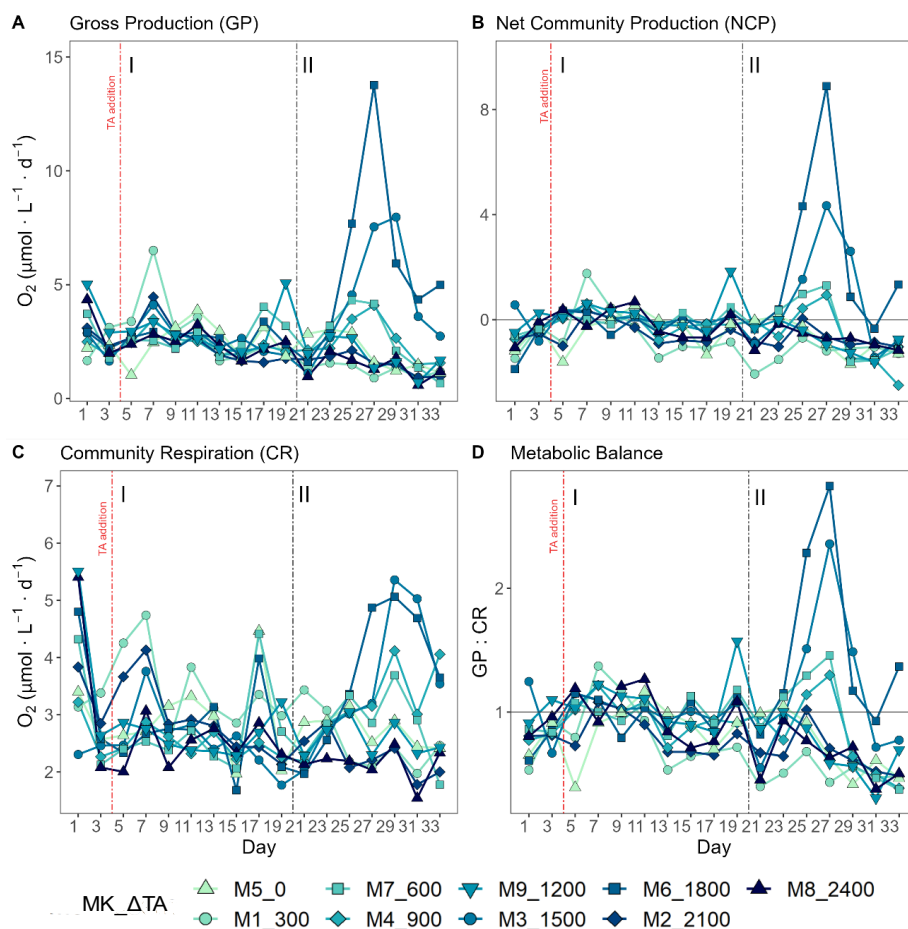
only for two days (Figure 2.B and D).

Figure 2. Results for metabolic rates measured through oxygen production and consumption showing A) the gross production (GP) temporal development, B) the net community production (NCP) temporal development, C) the community respiration (CR) temporal development, and E) the temporal development of the metabolic balance (GCP over CR). In the legend, MK corresponds to Mesocosm and TA to Total Alkalinity.

285

Phase-averaged linear regressions with the whole TA gradient revealed no significant treatment effect

(alpha < 0.05) on NCP, GP, and CR rates as well as metabolic balance (GP:CR) (Supp. Fig. S3).

Additionally, no impact of the abiotic precipitation in the highest treatment was observed regarding GP,

NCP, CR, GP:CR (Figure 2), ^{14}C primary production, and Chl$a$ concentration (Figure 3 and 4).
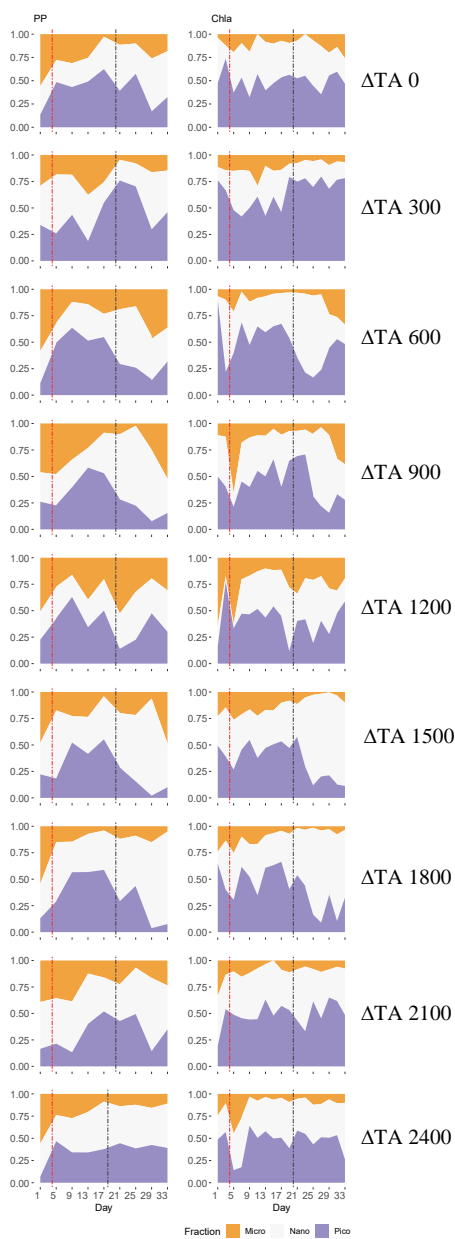
Figure 3. Temporal development of the three phytoplankton size fractions' (pico 0.2-2 µm; nano 2-20 µm; micro >20 µm) relative contributions to primary production (PP) through ^{14}C uptake (left column) and chlorophyll a (Chla) concentration (right column), for each treatment

290

In terms of relative contribution of pico, nano and micro to PP and Chl$a$, differences between phases are only clear in the Δ600, Δ900, Δ1800 and Δ2100 treatments, those that showed autotrophy (Figure 2D) in the second phase (Figure 3). In these mesocosms, pico, and in Δ900 micro also in terms of PP (Figure 3,

10

left), contributed the most in the first phase. However, in the second phase, nano became more dominant in
these intermediate treatments, especially in Δ1500 and Δ1800, and except in Δ1200, in which the micro
fraction contributed more throughout as compared to the other treatments. Total PP and Chl*a* concentration
data matched the spike in oxygen production observed in treatments Δ1500 and Δ1800, and also the slight
increases found in treatments Δ600 and Δ900 (Figure 4). Data for PP on day 27 were not collected. Thus,
the peak in Δ1800 reflected by the Chl*a* (Figure 4A and B), and the GCP and NCP rates (Figure 2), which
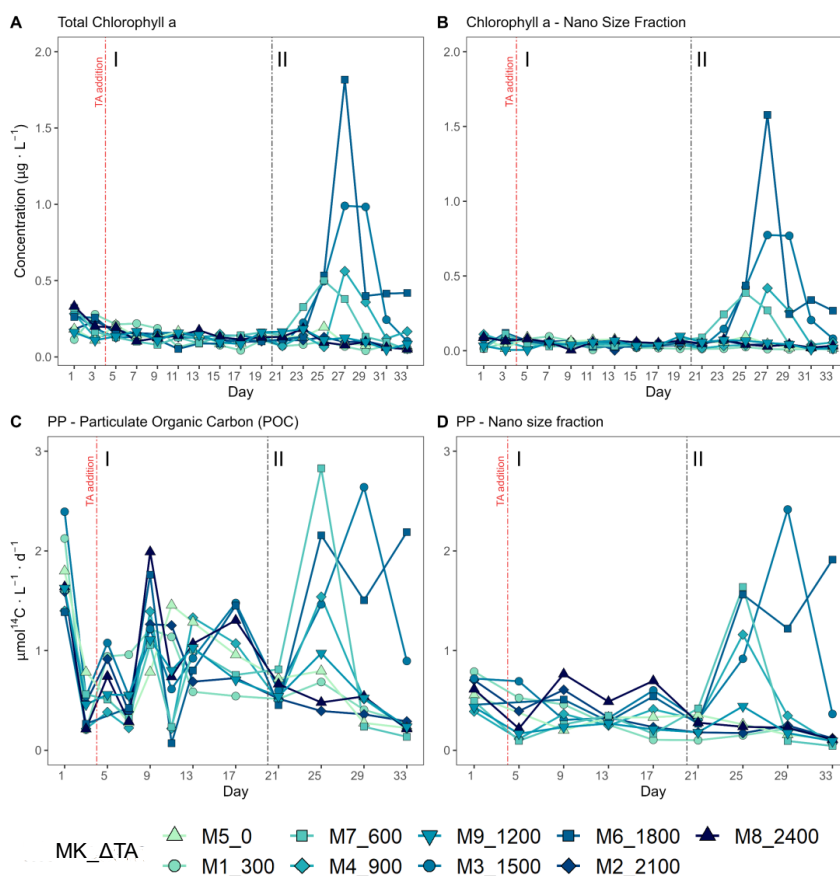was higher than in Δ1500, was excluded (Figure 4C and D).

**Figure 4. Temporal development of A) Chla concentration C) total particulate organic carbon
production and (left column), and of the nanophytoplankton fraction's contributions (right column) to
B) Chla concentration and to D) PP-total. MK corresponds to Mesocosm and TA to Total Alkalinity.**

The peaks in production observed in phase II were driven by nanophytoplankton growth (Figure 3, 4.B &
D). When considering all treatments, in phase I this size fraction showed a positive linear trend in relation
to the alkalinity ($R^2 = 0.51$; $p = 0.031$) and the DIC ($R^2 = 0.50$; $p = 0.031$) gradients in terms of ^{14}C uptake.
However, this significant relationship vanished by phase II.

Regarding Percent of Extracellular organic carbon Release (PER), no statistically significant linear relationship with the whole DIC gradient was found (Figure 5). Moreover, and as is true for all other parameters presented in this study, PER behaved disparately during the two phases. For the intermediate treatments, where there was autotrophy in the second phase, PER values dropped in comparison to the two highest and two lowest treatments, while Δ1200 stayed the same. Additionally, if the two highest treatments are excluded from the analysis, a significant negative relationship between the PER and the DIC gradient can be observed (Figure 5).
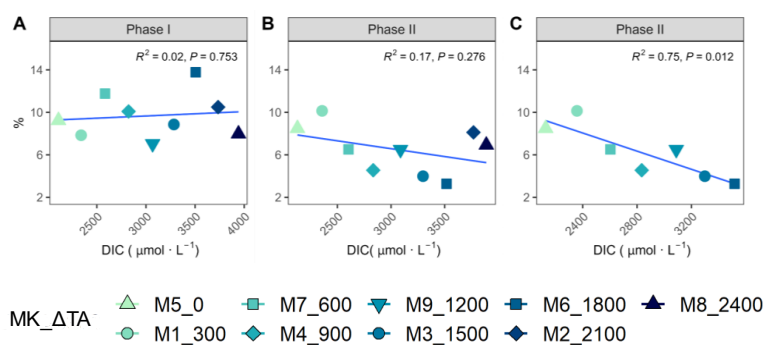

Figure 5. Linear regressions between ΔTA treatment and PER per phase (A. phase I and B. phase II), and (C) removing the two highest treatments in phase II. MK corresponds to Mesocosm and TA to Total Alkalinity.

3.3 Community Composition

Nanoeukaryote (1) abundance, despite gradually dropping throughout the experiment, showed a positive linear relationship ($R^2 = 0.634$, p= 0.01) with TA across both phases. Nanoeukaryote (2) abundance drove GP, NCP, and PP rates, and contributed the most to Chl*a* in the intermediate treatments, except Δ1200, during phase II (Figure 4 and 6). *Synechoccocus* proliferated in phase II in the lower intermediate treatments (treatments Δ600 and Δ900) as seen in Figure 6. Picoeukaryote abundance decreased during the first phase and picked back up 3-fold in the intermediate treatments from Δ600 to Δ1800. In addition, no impact of the indirect abiotic precipitation that occurred in the highest treatment during phase II was observed on any of the population abundances monitored (Figure 6). In fact, abundances of all groups in the latter treatment are comparable to those observed in the control.
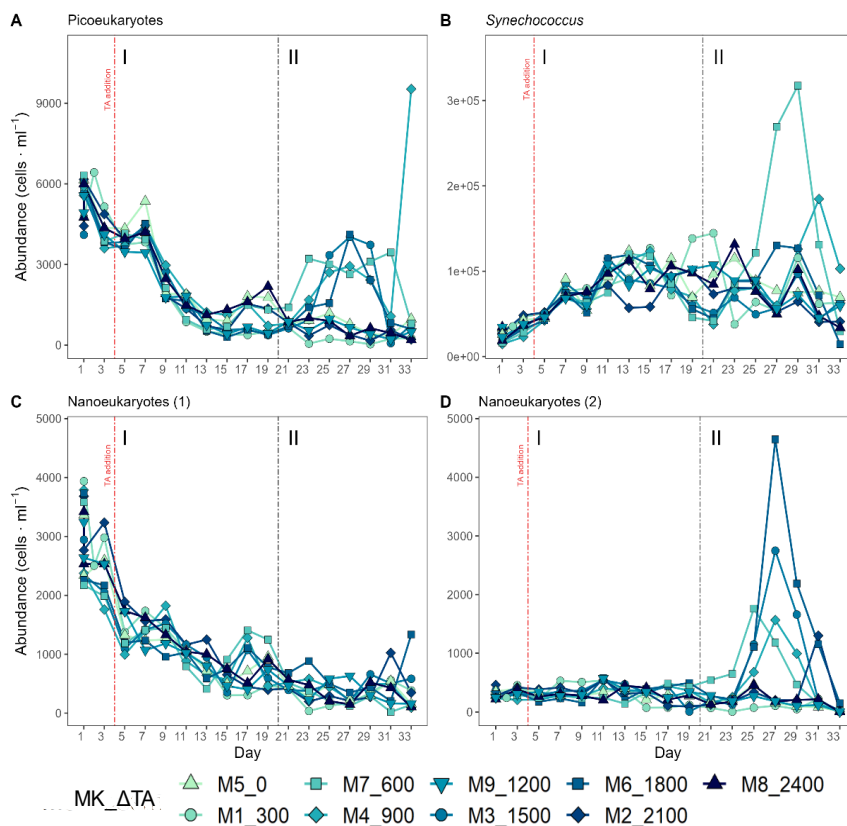
Figure 6. Abundance in cells m⁻¹ obtained through flow cytometry of A) picoeukaryotes, B) Synechococcus and C) and D) two nanoeukaryote populations. MK corresponds to Mesocosm and TA to Total Alkalinity.

335

3.4 Non-linear response vs no response

TA and DIC relate to each other (Supp. Fig. S4) and, if a potential non-linear response between the metabolic parameters listed in Table 2 were to be considered, the substrate in these relationships would most likely be DIC (key substrate for carbon fixation; Badger et al., 1998), not TA. The non-linear response

340 was detected for the longer-term phase, meaning the averaged-out values of phase II, but also of the entire duration of the experiment. Average GP and NCP rates, GP:CR, total PP, particulate and dissolved organic carbon (POC and DOC) production, and Chl$a$, the nanophytoplankton contribution to the latter two, and the nanoeukaryote abundances, all exhibited a gradual increase in the intermediate treatments, and a decline beyond ΔTA 1800 µmol · L⁻¹, during the mentioned time periods. Indeed, if the two highest treatments are

345 excluded from the model, significant linear relationships emerge between DIC, and all the parameters listed above for both phase II and the entire experiment (Table 2). However, it is worth noting that these relationships yield stronger regression coefficients when second-order polynomial regression models are employed instead (Table 2). Furthermore, a significant relationship is observed in phase I between NCP, metabolic balance and nanoeukaryote (2) abundance if the polynomial model is fitted (Table 2, left). Linear

350 relationships also become evident for the latter parameter when analyzed independently (Table 2, middle).

However, when linear regressions are employed and the two treatments with the highest responses ($\Delta1500$ and $\Delta1800$ µmol · L^{-1}) are excluded instead, the significance of all the previously described relationships is no longer observed (Table 2). Although, the nanophytoplankton contribution to PP in phase I and the nanoeukayote (1) abundance throughout the experiment continue to exhibit a significant linear trend, even

355   when these two intermediate treatments are excluded. This suggests that these specific relationships remain robust and significant, regardless of the exclusion of the highest-response treatments.

360

Table 2. Summary tables showing the regression coefficient values of (left) second order polynomial regression models, (middle) linear regression models, in both cases excluding the two highest treatments (Δ2100 and Δ2400 μmol · L⁻¹), and (right) linear models excluding the two treatments that show the highest response (Δ1500 and Δ1800 μmol · L⁻¹), fitted for gross and net community production (GP and NCP), metabolic balance (GP:CR), ¹⁴C Primary Production (PP-total, POC and DOC), the nanophytoplankton fraction contribution to PP_Total (PP_Nano), total Chla concentration (Chla), the nanophytoplankton fraction contribution to total Chla concentration (Chla_Nano), and the abundances of nanoeukaryotes (1) and (2) counted through flow cytometry, in relation to DIC. The p-values are indicated with the colour code (see legend).

y	Polynomial without 2 highest treatments [y ~ DIC + I(DIC^2)]			Linear without 2 highest treatments [y ~ DIC]			Linear without Δ1500 and Δ1800 treatments [y ~ DIC]		
	Phase I	Phase II	Throughout	Phase I	Phase II	Throughout	Phase I	Phase II	Throughout
GP	0.034	0.834	0.880	0.007	0.630	0.677	0.192	0.158	0.405
NCP	0.729	0.857	0.881	0.487	0.614	0.763	0.025	0.004	0.018
GP:CR	0.758	0.812	0.878	0.463	0.616	0.767	0.016	0.022	0.0005
PP_Total	0.527	0.705	0.791	0.002	0.618	0.532	0.091	0.130	0.001
PP_POC	0.538	0.703	0.806	0.008	0.620	0.561	0.085	0.118	0.005
PP_DOC	0.250	0.792	0.749	0.160	0.656	0.528	0.057	0.104	0.002
PP_Nano	0.588	0.752	0.788	0.369	0.644	0.371	0.474	0.048	0.096
Chla	0.176	0.783	0.782	0.128	0.667	0.668	0.110	0.039	0.029
Chla_Nano	0.243	0.779	0.785	0.148	0.653	0.643	0.039	0.028	0.023
Nano (1)	0.132	0.872	0.687	0.003	0.598	0.577	0.407	0.194	0.623
Nano (2)	0.723	0.658	0.696	0.683	0.576	0.623	0.015	0.0001	9.86E-06

p-value	0 - 0.001	0.001 - 0.01	0.01 - 0.05	0.05 - 0.1	0.1 - 1

365 The cross-validation test results indicate that the second polynomial term of DIC is marginally significant (p-value between 0.05 and 0.1) while the first polynomial term (the linear model) is statistically significant (p-values < 0.05). Although notably, both of these terms have a positive coefficient. Thus, suggesting that, even though the second polynomial term leads to higher regression coefficients, it may have a weaker although potentially relevant effect (still >90 % confidence level) on the response variable when compared to the linear model.

15

4. Discussion

370   The main goal of this study was to simulate an ocean liming OAE scenario. As a first step, carbonate based, CO_2 equilibrated solutions were used in order to simulate a best-case scenario. CO_2 equilibration, i.e., keeping pCO_2 levels constant, allows for greater alkalinity additions before the $CaCO_3$ saturation threshold is reached. The levels of exposure at an alkalinity dispersal plume were simulated through the ΔTA gradient. The oligotrophic waters surrounding the Canary Islands were chosen as an open ocean oligotrophic system

375   analog in terms of nutrient availability and community composition.

A neutral response of the measured metabolic rates, PP, Chl*a*, and community composition, when taking the entire alkalinity range applied here into account, was observed. These results are consistent with four-day microcosm experiments carried out at sea with two natural microbial communities of the North Atlantic subtropical gyre (Subhas et al., 2022). In this case, only 3 alkalinity treatments were deployed, with the

380   highest being ~ 4500 µmol kg^{-1}, and also using $NaHCO_3$ and Na_2CO_3 stock solutions. No major effect on the estimated net primary production, minor effects on community composition, and no influence on net calcification rates, were observed after 4 days. Results that, followed by those obtained from the current longer-term study, suggest this OAE approach may not entail significant alterations to microbial communities in oligotrophic pelagic systems.

385   However, nutrient limitation (Supp. Fig. S5) may have concealed more apparent responses to the TA and DIC gradients. In eutrophic environments, a transient positive impact on calcifiers, if present at the time of deployment, has been hypothesized due to the provision of additional substrate for calcification in the form of carbonate ions (Bach et al., 2019). Notably at and surrounding the alkalinity addition hotspot where the carbonate system is altered the most. Nevertheless, a recently published study showed no response of

390   *Emiliania huxleyi* to a limestone inspired alkalinity addition in a laboratory setting, with high nutrient availability, in terms of growth rates and elemental ratios after 6 days (Gately et al., 2023). Whether this is the case in a natural environment, and for longer term exposure to such conditions, is unknown. These results suggest that the effects of OAE on community structure and composition may be more complex than anticipated with the "green vs white" ocean hypothesis (Bach et al., 2019). However, further

395   experimental research is necessary to evaluate the consequences of, for instance, a silicate versus a carbonate based OAE deployment but also of OAE in more eutrophic environments. More specifically regarding community structure, calcification and silicification, but also primary production and metabolic balance, to address key knowledge gaps.

16

4.1 Potential for non-linear effects of OAE on metabolic rates

In the current study, a linear short-term response was observed for the nano fraction's contribution to PP,
and a positive relationship between nanoeukaryote (1) abundance and TA was detected when considering
the averages for the whole experiment. These results are supported by those obtained by Ferderer et al.
(2022). They reported a significant difference in the Chl$a$ concentrations, also driven by nanophytoplankton
growth, between the control and an equilibrated alkalinity treatment in a microcosm experiment. These
results suggest that certain nanophytoplankton species may benefit from the carbonate chemistry conditions
associated with CO_2 equilibrated OAE. Overall, however, in the present study, no significant linear
relationships with the whole TA gradient were found in any other parameter after a month-long exposure
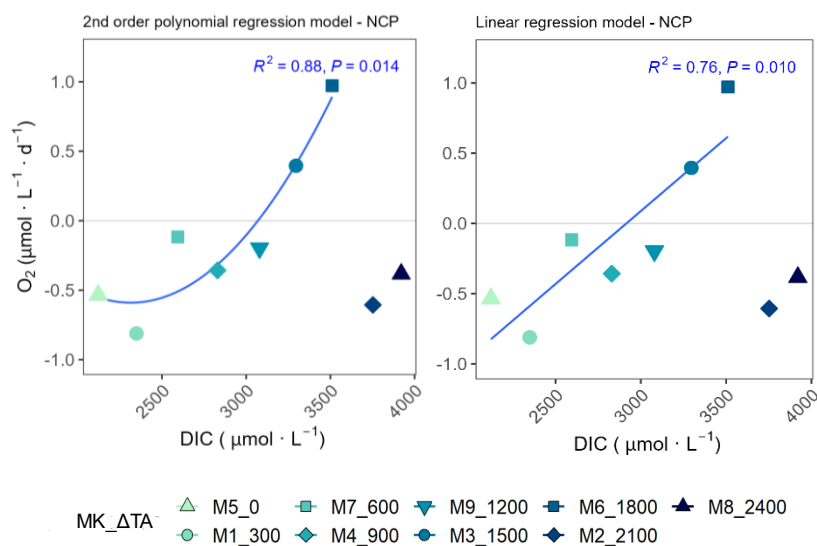to such conditions.

Figure 7. Second order polynomial (left) and linear (right) regression models fitted to the treatments of up to ΔTA1800 µmol · L^{-1} relating Net Community Production (NCP) Rates and the associated Dissolved Inorganic Carbon (DIC) levels averaged out for the whole experiment. In the legend, MK corresponds to Mesocosm and TA to Total Alkalinity.

Albeit at constant pCO_2, prolonged exposure to higher calcite/aragonite saturation states and moderate pH
increases in an OAE dispersal plume has been hypothesized to lead to nonlinear and/or threshold-like
responses in the long-term (Subhas et al., 2022). This pattern was noticed for the parameters listed in Table
2 in relation to DIC, suggesting there may in fact be an optimum curve-like response, and a threshold

17

between $\Delta1800$ and $\Delta2100$ µmol L^{-1} treatments (Figure 6). Indeed, if only the treatments below $\Delta2100$ µmol L^{-1} are considered, positive significant relationships, described by polynomial (higher regression coefficients) and linear regression models (Table 2 and Figure 7), arise between DIC and NCP, GP, GP:CR, PP-total, POC and DOC production, PP-Nano, total Chl*a,* Chl*a*-Nano, and both nanoeukaryote clusters'

420 abundances. In addition to the opposite pattern being reflected by the PER (Figure 7). PER is known to be higher in oligotrophic than in eutrophic waters (Chróst, 1983; Teira et al., 2001). The observed decrease in the PER associated to the OAE treatment up to $\Delta1800$ µmol L^{-1} in the second phase suggests a potential accumulation of inorganic nutrients, and thus that nitrogen cycle processes may have been affected too. In fact, the latter are known to be pH dependent (Beman et al., 2011; Fumasoli et al., 2017; Pommerening-

425 Röser & Koops, 2005). Paul, et al. (2023, in prep) observed a positive relationship of Particulate Organic Carbon to Particulate Organic Nitrogen (POC: PON) ratios in the second phase, and a negative relation of Particulate Organic Nitrogen (PON) concentrations in the first phase, both with the OAE treatment. Thus, considering that all the earlier described responses occurred in the second phase (designated as long term), the peak in production may have been possible due to a slight increase in heterotrophic turnover of organic

430 nitrogen associated to the carbonate chemistry manipulation, which would explain the lag in the observed responses.

Actually, considering the nutrient-depleted nature of the system in all mesocosms, the occurrence of the peaks in production that drive the optimum curve-like relationship was unexpected. All that is currently known about the species responsible for the increase in productivity observed in the four intermediate

435 treatments (Figure 7) is that it was a *Chrysochromulina* spp. In a study carried out from May to June 1988 in the Kattegat, *C. polylepis* was monitored prior to the decline of a bloom (Kaas et al., 1991). The authors measured its distribution, primary production, and nitrogen dynamics and found that *C. polylepis* showed high affinity for ammonia. It was its main nitrogen source and the only nutrient that was not measured in the current study.

440 An alternative explanation could be that the protagonist in the intermediate treatments during the second phase of the experiment was *C. parkeae,* which is a life cycle stage of *Braarudosphaera bigelowii* (Suzuki et al., 2021). The latter is known to possess a nitrogen fixing cyanobacterial endosymbiont (UCYN-A; Suzuki et al., 2021) that would have allowed it to adapt to the highly nutrient depleted environment. In addition, *B. bigelowii* is a haptophyte that was found to perform extracellular calcification (Hagino et al.,

445 2016) and thus, may have benefited from the increase in the calcite saturation state.

18

Taxon-specific, optimum curve-like responses of phytoplankton growth to the combined effect of H^+ and CO_2 have previously been reported (Paul & Bach, 2020). CO_2 is usually considered the main source of carbon for primary production. However, most marine phytoplankton are capable of actively taking up bicarbonate thanks to carbon concentrating mechanisms (CCMs; Giordano et al., 2005; Price et al., 2008).

450   Bicarbonate ions are accumulated in the cytosol, and later converted to CO_2 prior to carboxylation (Price et al., 2008). In the present study DIC was increased according to an equilibrated (no reduction in CO_2) TA gradient. This manipulation was the main difference between the mesocosms. Thus, the bicarbonate availability levels attained in the intermediate treatments, where autotrophy was observed, may have been behind the detected peaks in production, alongside the potential relief of nutrient limitation explained

455   above. Meaning that, in the current experiment, a certain nanophytoplankton species with more evolved CCMs may have benefited from the higher DIC concentrations, and slight pH increase, directly and indirectly respectively.

Chi et al. (2014) studied different strains of microalgae and cyanobacteria as candidates for bicarbonate-based carbon capture for algae production (BICCAPS). Depending on the species, different growth rates

460   and thresholds, and in some cases growth inhibition, were observed when these were cultured under varying bicarbonate concentrations. This is due to their ion strength tolerance and may explain the potential threshold found in the current study.

However, whether the peaks observed in $\Delta1500$ and $\Delta1800$ $\mu mol \cdot L^{-1}$, that drive the detected optimum curve (Table 2 and Figure 7) occurred by random chance and were thus not caused by the carbonate

465   chemistry conditions, remains unclear. In fact, when removing $\Delta1500$ and $\Delta1800$ $\mu mol \cdot L^{-1}$ from the model instead of the two highest treatments, these positive significant relationships with DIC vanish (Table 2). Although, these nutrient-decoupled peaks in production only occurred in mesocosms where TA, DIC and, to a lesser extent pH, were increased. It is a novel sighting since a response of this magnitude has not been observed in previous experiments carried out under nutrient depleted conditions, and/or while testing ocean

470   acidification, in the Canary Islands (Paul, et al., 2023: in prep). Consequently, and also considering the results from the cross-validation test, additional studies simulating the gradient applied here or similar, though with replicates, could further elucidate if such a threshold and the positive relation found below it hold.

475   **4.2 Challenges and limitations of OAE studies**

19

A limitation of this experimental set up that should also be mentioned is that mesocosm studies are limited to temporal scales of weeks to months, precluding the study of potential longer-term effects. Additionally, secondary precipitation in the highest treatment likely occurred due to the substrate for nuclei formation provided by the mesocosm walls themselves, although it may not be the sole cause.

480   Hartmann et al. (2023) carried out CO_2 equilibrated alkalinity additions of up to $\Delta 2400$ µmol L^{-1} using the same stock solutions as in our experiment. Biotic incubations that included phytoplankton and particles smaller than 55 µm, which are potential seed surface for nucleation, were set up. They observed no precipitates forming on the bottle walls, and thus no TA consumption, after 4 days. However, in their long-term, up to 90-day alkalinity stability experiment, precipitation was observed in the "untreated mode" (or

485   control, meaning no particle addition), 10 days after the TA increase. Hartmann et al. (2023) hypothesized that precipitation was potentially triggered by the wall-effect since it was an abiotic treatment containing no particles larger than 0.2 µm. Furthermore, when precipitates from other experiments were added to the "treated mode" treatments, immediate and persistent precipitation was observed for both $\Delta 2100$ and $\Delta 2400$ µmol L^{-1}. Additionally, Wurgaft et al., (2021) found that TA loss via abiotic precipitation occurred at lower

490   levels in a natural system than in these experiments due to the sediment particles in river plumes.

Thus, the secondary precipitation observed in the present study, as previously stated, may have been due to a combination of the wall-effect, including cleaning procedures that caused resuspension of particles present on the walls, but also to the existence of particles and cells in the water column. Whether carbonate formation would occur around the levels (~ 4500 µmol $\cdot L^{-1}$) observed in this study in a natural oligotrophic,

495   open ocean environment is still unclear. Actually, the theoretical aragonite saturation (Ω_{Ar}) threshold of 12.5 above which carbonate precipitation was expected to occur (Morse and He, 1993), was never surpassed (Table 1).

4.3 Implications for future OAE research

500   Further experimental research at this scale is essential to test the effects of non-equilibrated OAE approaches as well. These may be more viable considering the current infrastructure since large scale equilibrated OAE application may require the use of reactors to CO_2 equilibrate the alkaline solutions prior to addition (Hartmann et al., 2023).

At the alkalinity point source, and depending on the alkalinity dispersal plume dynamics, the carbonate

505   system perturbations associated to non-equilibrated OAE can be much stronger. Alkalinity loss would also be triggered at much lower levels than those observed for CO_2 equilibrated OAE (Hartmann et al., 2023).

Besides, when precipitation is triggered, a process by which precipitation keeps progressing past reaching the aragonite saturation levels of 12.5-13.5, and even ambient levels, also known as "runaway precipitation" (Moras et al., 2022), may be induced.

510 The findings of the current study suggest that carbonate-based, CO_2 equilibrated OAE may be environmentally safe in terms of the metabolic processes measured here, in an oligotrophic environment, even if abiotic precipitation were triggered. Although further research is required on the impacts of this phenomenon on other processes, i.e. on particle sinking due to ballasting. Moreover, uncertainty remains in the determination of responses to longer term exposure to the conditions simulated in this study, and in

515 the levels at which abiotic precipitation may occur in the natural open ocean.

Several risks and co-benefits have been listed for this NET (Bach et al., 2019;), although none have been really tested at a reasonable scale. This study concludes there may be a potential co-benefit to the addition of carbonates in solution, with CO_2 equilibration, where biological carbon sequestration is increased up to a certain threshold. Moreover, and as is true for ocean acidification, this response is species/group specific.

520 In addition, past the mentioned threshold, production decreased but rates were comparable to those measured for the control and $\Delta300$ µmol · L^{-1} treatments. Therefore, no impact of equilibrated OAE past the ~4000 µmol · L^{-1} TA threshold, and of abiotic precipitation at ~4300 µmol · L^{-1}, on the measured metabolic rates can be inferred.

525 **5. Conclusions**

An ideal Ocean Alkalinity Enhancement (OAE) deployment scenario was simulated under natural conditions. Total alkalinity (TA) was increased without the introduction of potentially harmful dissolution by-products, and CO_2 was chemically sequestered prior to the TA manipulation. The OAE approach employed within the specified TA range did not pose a threat to the pelagic microbial community in relation

530 to the parameters monitored in the current study. Importantly, this held true even when abiotic precipitation occurred in the highest treatment. Only minor changes in species composition were observed. In fact, we observed a potential co-benefit in the form of increased microbial community production, possibly driven by enhanced nitrogen cycling. Our discovery of a non-linear, optimal curve-like response in microbial production rates to the applied Dissolved Inorganic Nitrogen (DIC) gradient (as shown in Table 2) is

535 noteworthy and suggests potential influence from carbonate chemistry conditions and increased heterotrophic turnover rates of organic nitrogen. This finding is novel and warrants further investigation. Therefore, additional research on carbon uptake efficiency and the effects of CO_2, but also non-CO_2

equilibrated OAE on natural microbial communities is of high priority, considering the substantial climatic benefits it could offer.

540

Data availability

The raw data supporting the conclusions of this article will be made available by the authors, without undo reservation.

545 **Author contributions**

Experimental concept and design: UR and JA. Execution of the experiment: All authors. Data analysis: LMS with input from NHH and JO. Original draft preparation: LMS. Review and editing: All authors.

Competing interests

The authors declare that they have no conflict of interest.

560

22

References

575   Bach, L. T., Gill, S. J., Rickaby, R. E. M., Gore, S., & Renforth, P. (2019). CO2 Removal With Enhanced
        Weathering and Ocean Alkalinity Enhancement: Potential Risks and Co-benefits for Marine Pelagic
        Ecosystems. *Frontiers in Climate*, *1*(October). https://doi.org/10.3389/fclim.2019.00007

Badger, M. R., Andrews, T. J., Whitney, S. M., Ludwig, M., Yellowlees, D. C., Leggat, W., & Price, G. D.
        (1998). The diversity and coevolution of Rubisco, plastids, pyrenoids, and chloroplast-based CO2-

580   concentrating   mechanisms   in   algae.   *Canadian   Journal   of   Botany*,   *76*(6),   1052–1071.
        https://doi.org/10.1139/b98-074

Beman, J. M., Chow, C. E., King, A. L., Feng, Y., Fuhrman, J. A., Andersson, A., Bates, N. R., Popp, B.
        N., & Hutchins, D. A. (2011). Global declines in oceanic nitrification rates as a consequence of ocean
        acidification. *Proceedings of the National Academy of Sciences of the United States of America*,

585   *108*(1), 208–213. https://doi.org/10.1073/pnas.1011053108

Burns, W., & Corbett, C. R. (2020). Antacids for the Sea? Artificial Ocean Alkalinization and Climate
        Change. *One Earth*, *3*(2), 154–156. https://doi.org/10.1016/j.oneear.2020.07.016

Butenschön, M., Lovato, T., Masina, S., Caserini, S., & Grosso, M. (2021). Alkalinization Scenarios in the
        Mediterranean Sea for Efficient Removal of Atmospheric CO2 and the Mitigation of Ocean

590   Acidification. *Frontiers in Climate*, *3*(March), 1–11. https://doi.org/10.3389/fclim.2021.614537

Carpenter, C. and. (1966). *Modifications Employed of the Winkler Method for Determining Dissolved
        Oxygen in Seawater ; A NASCO Report '*.

Caserini, S., Pagano, D., Campo, F., Abbà, A., De Marco, S., Righi, D., Renforth, P., & Grosso, M. (2021).
        Potential of Maritime Transport for Ocean Liming and Atmospheric CO2 Removal. *Frontiers in*

595   *Climate*, *3*(April), 1–18. https://doi.org/10.3389/fclim.2021.575900

Chen, C. Y., Durbin, E. G., Marine, S., Progress, E., & June, N. (1994). *Effects of pH of marine on t phy*.
        109(1), 83–94.

Chen, S. M., Riebesell, U., Schulz, K. G., Von Der Esch, E., Achterberg, E. P., & Bach, L. T. (2022).
        Temporal dynamics of surface ocean carbonate chemistry in response to natural and simulated

600   upwelling events during the 2017 coastal El Niño near Callao, Peru. *Biogeosciences*, *19*(2), 295–312. https://doi.org/10.5194/bg-19-295-2022

Chi, Z., Elloy, F., Xie, Y., Hu, Y., & Chen, S. (2014). Selection of microalgae and cyanobacteria strains for bicarbonate-based integrated carbon capture and algae production system. *Applied Biochemistry and Biotechnology*, *172*(1), 447–457. https://doi.org/10.1007/s12010-013-0515-5

605   Chróst, R. J. (1983). Plankton photosynthesis, extracellular release and bacterial utilization of released dissolved organic carbon (RDOC) in lakes of different trophy. *Acta Microbiologica Polonica*, *32*(3), 275–287.

Dubelaar, G. B. J., & Gerritzen, P. L. (2000). CytoBuoy: A step forward towards using flow cytometry in operational oceanography. *Scientia Marina*, *64*(2), 255–265.
610   https://doi.org/10.3989/scimar.2000.64n2255

Eisaman, M. D., Geilert, S., Renforth, P., Bastianini, L., Campbell, J., Dale, W., Foteinis, S., Grasse, P., Hawrot, O., Löscher, C. R., & Rau, G. H. (2023). *Chapter 3 : Assessing the technical aspects of OAE approaches*. *June*, 1–52.

Feely, R. A., Sabine, C. L., Lee, K., Berelson, W., Kleypas, J., Fabry, V. J., & Millero, F. J. (1985). Impact
615   of Anthropogenic CO_2 on the $CaCO_3$ System in the Oceans. *Journal of Agronomic Education*, *14*(1), 3–7. https://doi.org/10.2134/jae1985.0003

Feng, E. Y., Koeve, W., Keller, D. P., & Oschlies, A. (2017). Model-Based Assessment of the CO_2 Sequestration Potential of Coastal Ocean Alkalinization. *Earth's Future*, *5*(12), 1252–1266. https://doi.org/10.1002/2017EF000659

620   Ferderer, A., Chase, Z., Kennedy, F., Schulz, K. G., & Bach, L. T. (2022). Assessing the influence of ocean alkalinity enhancement on a coastal phytoplankton community. *Biogeosciences*, *19*(23), 5375–5399. https://doi.org/10.5194/bg-19-5375-2022

Friedlingstein, P., Jones, M. W., O'Sullivan, M., Andrew, R. M., Bakker, D. C. E., Hauck, J., Le Quéré, C., Peters, G. P., Peters, W., Pongratz, J., Sitch, S., Canadell, J. G., Ciais, P., Jackson, R. B., Alin, S.
625   R., Anthoni, P., Bates, N. R., Becker, M., Bellouin, N., … Zeng, J. (2022). Global Carbon Budget 2021. *Earth System Science Data*, *14*(4), 1917–2005. https://doi.org/10.5194/essd-14-1917-2022

Fumasoli, A., Bürgmann, H., Weissbrodt, D. G., Wells, G. F., Beck, K., Mohn, J., Morgenroth, E., & Udert, K. M. (2017). Growth of Nitrosococcus-Related Ammonia Oxidizing Bacteria Coincides with Extremely Low pH Values in Wastewater with High Ammonia Content. *Environmental Science and*
630   *Technology*, *51*(12), 6857–6866. https://doi.org/10.1021/acs.est.7b00392

Gafar, N. A., & Schulz, K. G. (2018). A three-dimensional niche comparison of Emiliania huxleyi and Gephyrocapsa oceanica: Reconciling observations with projections. *Biogeosciences*, *15*(11), 3541–3560. https://doi.org/10.5194/bg-15-3541-2018

635 Gately, J. A., Kim, S. M., Jin, B., Brzezinski, M. A., & Iglesias-rodriguez, M. D. (2023). *Coccolithophores and diatoms resilient to ocean alkalinity enhancement: A glimpse of hope? 6066.* https://doi.org/10.1126/sciadv.adg6066

Gattuso, J. P., Magnan, A. K., Bopp, L., Cheung, W. W. L., Duarte, C. M., Hinkel, J., Mcleod, E., Micheli, F., Oschlies, A., Williamson, P., Billé, R., Chalastani, V. I., Gates, R. D., Irisson, J. O., Middelburg, J. J., Pörtner, H. O., & Rau, G. H. (2018). Ocean solutions to address climate change and its effects
640 on marine ecosystems. *Frontiers in Marine Science*, *5*(OCT). https://doi.org/10.3389/fmars.2018.00337

Gattuso, J. P., Williamson, P., Duarte, C. M., & Magnan, A. K. (2021). The Potential for Ocean-Based Climate Action: Negative Emissions Technologies and Beyond. *Frontiers in Climate*, *2*(January), 1–8. https://doi.org/10.3389/fclim.2020.575716

645 Giordano, M., Beardall, J., & Raven, J. A. (2005). CO2 concentrating mechanisms in algae: Mechanisms, environmental modulation, and evolution. *Annual Review of Plant Biology*, *56*, 99–131. https://doi.org/10.1146/annurev.arplant.56.032604.144052

Goldenberg, S. U., Taucher, J., Fernández-Méndez, M., Ludwig, A., Arístegui, J., Baumann, M., Ortiz, J., Stuhr, A., & Riebesell, U. (2022). Nutrient composition (Si:N) as driver of plankton communities
650 during artificial upwelling. *Frontiers in Marine Science*, *9*(November), 1–15. https://doi.org/10.3389/fmars.2022.1015188

González, M. F., & Ilyina, T. (2016). Impacts of artificial ocean alkalinization on the carbon cycle and climate in Earth system simulations. *Geophysical Research Letters*, *43*(12), 6493–6502. https://doi.org/10.1002/2016GL068576

655 Grasshof, K., Kremling, K., & Ehrhard, M. (1999). Arsenic , antimony , and germanium , in Methods of Seawater Analysis edited. *Wiley-VCH, Weinheim*, *May*, 274–294.

Hagino, K., Tomioka, N., Young, J. R., Takano, Y., Onuma, R., & Horiguchi, T. (2016). Extracellular calcification of Braarudosphaera bigelowii deduced from electron microscopic observations of cell surface structure and elemental composition of pentaliths. *Marine Micropaleontology*, *125*, 85–94.
660 https://doi.org/10.1016/j.marmicro.2016.04.002

Hartmann, J., Suitner, N., Lim, C., Schneider, J., Marín-Samper, L., Arístegui, J., Renforth, P., Taucher, J.,

& Riebesell, U. (2023). Stability of alkalinity in ocean alkalinity enhancement (OAE) approaches - consequences for durability of CO2storage. *Biogeosciences*, *20*(4), 781–802. https://doi.org/10.5194/bg-20-781-2023

665   Harvey, L. D. D. (2008). Mitigating the atmospheric CO2 increase and ocean acidification by adding limestone powder to upwelling regions. *Journal of Geophysical Research: Oceans*, *113*(4), 1–21. https://doi.org/10.1029/2007JC004373

Haszeldine, R. S., Flude, S., Johnson, G., & Scott, V. (2018). Negative emissions technologies and carbon capture and storage to achieve the Paris Agreement commitments. *Philosophical Transactions of the*
670   *Royal Society A: Mathematical, Physical and Engineering Sciences*, *376*(2119). https://doi.org/10.1098/rsta.2016.0447

Hendriks, I. E., & Duarte, C. M. (2010). Ocean acidification: Separating evidence from judgment - A reply to Dupont et al. *Estuarine, Coastal and Shelf Science*, *89*(2), 186–190. https://doi.org/10.1016/j.ecss.2010.06.007

675   Ilyina, T., Wolf-Gladrow, D., Munhoven, G., & Heinze, C. (2013). Assessing the potential of calcium-based artificial ocean alkalinization to mitigate rising atmospheric CO2 and ocean acidification. *Geophysical Research Letters*, *40*(22), 5909–5914. https://doi.org/10.1002/2013GL057981

IPCC. (2018). Global warming of 1.5°C. In *Special Report on Global Warming of 1.5°C*.

IPCC. (2022). Climate Change 2022: Mitigation of Climate Change. Contribution of Working Group III to
680   the Sixth Assessment Report of the Intergovernmental Panel on Climate Change. In *Cambridge University Press* (Issue 1). https://www.ipcc.ch/report/ar6/wg3/

Kaas, H., Larsen, J., Mohlenberg, F., & Richardson, K. (1991). The Chrysochromulina polylepis bloom in the Kattegat (Scandinavia) May-June 1988. Distribution, primary production and nutrient dynamics in the late stage of the bloom. *Marine Ecology Progress Series*, *79*(1–2), 151–161.
685   https://doi.org/10.3354/meps079151

Kheshgi, H. S. (1995). Sequestering atmospheric carbon dioxide by increasing ocean alkalinity. *Energy*, *20*(9), 915–922. https://doi.org/10.1016/0360-5442(95)00035-F

Köhler, P., Abrams, J. F., Völker, C., Hauck, J., & Wolf-Gladrow, D. A. (2013). Geoengineering impact of open ocean dissolution of olivine on atmospheric CO2, surface ocean pH and marine biology.
690   *Environmental Research Letters*, *8*(1). https://doi.org/10.1088/1748-9326/8/1/014009

Kroeker, K. J., Kordas, R. L., Crim, R., Hendriks, I. E., Ramajo, L., Singh, G. S., Duarte, C. M., & Gattuso, J. P. (2013). Impacts of ocean acidification on marine organisms: Quantifying sensitivities and

interaction with warming. *Global Change Biology*, *19*(6), 1884–1896. https://doi.org/10.1111/gcb.12179

695 Kroeker, K. J., Kordas, R. L., Crim, R. N., & Singh, G. G. (2010). Meta-analysis reveals negative yet variable effects of ocean acidification on marine organisms. *Ecology Letters*, *13*(11), 1419–1434. https://doi.org/10.1111/j.1461-0248.2010.01518.x

Lenton, A., Matear, R. J., Keller, D. P., Scott, V., & Vaughan, N. E. (2018). Assessing carbon dioxide removal through global and regional ocean alkalinization under high and low emission pathways.

700 *Earth System Dynamics*, *9*(2), 339–357. https://doi.org/10.5194/esd-9-339-2018

Lewis, E., & Wallace, D. (1998). *Program Developed for CO2 System Calculations ORNL/CDIAC-105, Carbon Dioxide Information Analysis Centre,* (pp. 1–29).

Lueker, T. J., Dickson, A. G., & Keeling, C. D. (2000). Ocean pCO2 calculated from dissolved inorganic carbon, alkalinity, and equations for K1 and K2: Validation based on laboratory measurements of

705 CO2 in gas and seawater at equilibrium. *Marine Chemistry*, *70*(1–3), 105–119. https://doi.org/10.1016/S0304-4203(00)00022-0

Moras, C. A., Bach, L. T., Cyronak, T., Joannes-Boyau, R., & Schulz, K. G. (2022). Ocean alkalinity enhancement - avoiding runaway CaCO3 precipitation during quick and hydrated lime dissolution. *Biogeosciences*, *19*(15), 3537–3557. https://doi.org/10.5194/bg-19-3537-2022

710 Orr, J. C., Fabry, V. J., Aumont, O., Bopp, L., Doney, S. C., Feely, R. A., Gnanadesikan, A., Gruber, N., Ishida, A., Joos, F., Key, R. M., Lindsay, K., Maier-Reimer, E., Matear, R., Monfray, P., Mouchet, A., Najjar, R. G., Plattner, G. K., Rodgers, K. B., … Yool, A. (2005). Anthropogenic ocean acidification over the twenty-first century and its impact on calcifying organisms. *Nature*, *437*(7059), 681–686. https://doi.org/10.1038/nature04095

715 Paul, A. J., & Bach, L. T. (2020). Universal response pattern of phytoplankton growth rates to increasing CO2. *New Phytologist*, *228*(6), 1710–1716. https://doi.org/10.1111/nph.16806

Pommerening-Röser, A., & Koops, H. P. (2005). Environmental pH as an important factor for the distribution of urease positive ammonia-oxidizing bacteria. *Microbiological Research*, *160*(1), 27–35. https://doi.org/10.1016/j.micres.2004.09.006

720 Price, G. D., Badger, M. R., Woodger, F. J., & Long, B. M. (2008). Advances in understanding the cyanobacterial CO2-concentrating- mechanism (CCM): Functional components, Ci transporters, diversity, genetic regulation and prospects for engineering into plants. *Journal of Experimental Botany*, *59*(7), 1441–1461. https://doi.org/10.1093/jxb/erm112

Rau, G. H., McLeod, E. L., & Hoegh-Guldberg, O. (2012). The need for new ocean conservation strategies in a high-carbon dioxide world. *Nature Climate Change*, *2*(10), 720–724. https://doi.org/10.1038/nclimate1555

Renforth, P., Jenkins, B. G., & Kruger, T. (2013). Engineering challenges of ocean liming. *Energy*, *60*, 442–452. https://doi.org/10.1016/j.energy.2013.08.006

Riebesell, U., Wolf-Gladrow, D. A., & Smetacek, V. (1993). Carbon dioxide limitation of marine phytoplankton growth rates. *Nature*, *361*(6409), 249–251. https://doi.org/10.1038/361249a0

Subhas, A. V., Marx, L., Reynolds, S., Flohr, A., Mawji, E. W., Brown, P. J., & Cael, B. B. (2022). Microbial ecosystem responses to alkalinity enhancement in the North Atlantic Subtropical Gyre. *Frontiers in Climate*, *4*. https://doi.org/10.3389/fclim.2022.784997

Suzuki, S., Kawachi, M., Tsukakoshi, C., Nakamura, A., Hagino, K., Inouye, I., & Ishida, K. I. (2021). Unstable Relationship Between Braarudosphaera bigelowii (= Chrysochromulina parkeae) and Its Nitrogen-Fixing Endosymbiont. *Frontiers in Plant Science*, *12*(December). https://doi.org/10.3389/fpls.2021.749895

Taucher, J., Bach, L. T., Boxhammer, T., Nauendorf, A., Achterberg, E. P., Algueró-Muñiz, M., Arístegui, J., Czerny, J., Esposito, M., Guan, W., Haunost, M., Horn, H. G., Ludwig, A., Meyer, J., Spisla, C., Sswat, M., Stange, P., Riebesell, U., Aberle-Malzahn, N., … Zark, M. (2017). Influence of ocean acidification and deep water upwelling on oligotrophic plankton communities in the subtropical North Atlantic: Insights from an in situ mesocosm study. *Frontiers in Marine Science*, *4*(APR). https://doi.org/10.3389/fmars.2017.00085

Teira, E., Pazó, M. J., Serret, P., & Fernández, E. (2001). Dissolved organic carbon production by microbial populations in the Atlantic Ocean. *Limnology and Oceanography*, *46*(6), 1370–1377. https://doi.org/10.4319/lo.2001.46.6.1370

Welschmeyer, N. A. (1994). Fluorometric analysis of chlorophyll a in the presence of chlorophyll b and pheopigments. *Limnology and Oceanography*, *39*(8), 1985–1992. https://doi.org/10.4319/lo.1994.39.8.1985

Wittmann, A. C., & Pörtner, H. O. (2013). Sensitivities of extant animal taxa to ocean acidification. *Nature Climate Change*, *3*(11), 995–1001. https://doi.org/10.1038/nclimate1982

Wurgaft, E., Wang, Z. A., Churchill, J. H., Dellapenna, T., Song, S., Du, J., Ringham, M. C., Rivlin, T., & Lazar, B. (2021). Particle Triggered Reactions as an Important Mechanism of Alkalinity and Inorganic Carbon Removal in River Plumes. *Geophysical Research Letters*, *48*(11), 1–10.

755   https://doi.org/10.1029/2021GL093178